

## **UC Davis**

### **UC Davis Previously Published Works**

**Title**

In situ electrical modulation and monitoring of nanoporous gold morphology

**Permalink**

<https://escholarship.org/uc/item/7cf0n5zj>

**Journal**

Nanoscale, 8(47)

**ISSN**

2040-3364

**Authors**

Dorofeeva, Tatiana S  
Seker, Erkin

**Publication Date**

2016-12-01

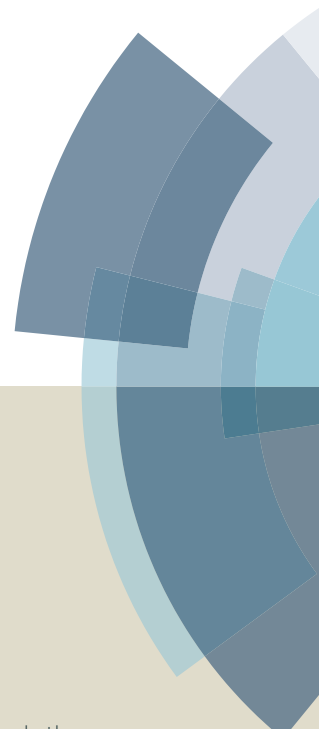
**DOI**

10.1039/c6nr07237b

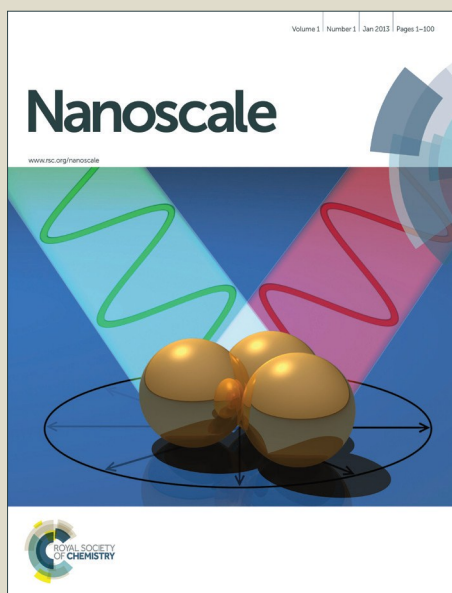
Peer reviewed

# Nanoscale

Accepted Manuscript



This article can be cited before page numbers have been issued, to do this please use: T. S. Dorofeeva and E. Seker, *Nanoscale*, 2016, DOI: 10.1039/C6NR07237B.



This is an *Accepted Manuscript*, which has been through the Royal Society of Chemistry peer review process and has been accepted for publication.

*Accepted Manuscripts* are published online shortly after acceptance, before technical editing, formatting and proof reading. Using this free service, authors can make their results available to the community, in citable form, before we publish the edited article. We will replace this *Accepted Manuscript* with the edited and formatted *Advance Article* as soon as it is available.

You can find more information about *Accepted Manuscripts* in the [Information for Authors](#).

Please note that technical editing may introduce minor changes to the text and/or graphics, which may alter content. The journal's standard [Terms & Conditions](#) and the [Ethical guidelines](#) still apply. In no event shall the Royal Society of Chemistry be held responsible for any errors or omissions in this *Accepted Manuscript* or any consequences arising from the use of any information it contains.

## In Situ Electrical Modulation and Monitoring of Nanoporous Gold Morphology

Tatiana S. Dorofeeva<sup>a</sup> and Erkin Seker<sup>a</sup>

Received 00th January 20xx,  
Accepted 00th January 20xx

DOI: 10.1039/x0xx00000x

[www.rsc.org/](http://www.rsc.org/)

The ability to fine-tune feature size in nanostructured thin films is critical, as many desirable properties of these materials are dictated by their nanostructure. Accordingly, there is a need for techniques that allow for modifying nanostructure while monitoring the morphological changes in situ. Here, we demonstrate a closed-loop electro-annealing system which enables in situ monitoring of morphology evolution in sub-micron nanoporous gold (np-Au) thin films. np-Au is produced by a microfabrication-compatible self-assembly process that produces a network of interconnected ligaments with tunable diameter (10s to 100s of nanometers), making it a desirable material for numerous applications and fundamental studies alike. We specifically investigate the relationship between np-Au morphology (i.e., ligament diameter) and electrical resistance of the thin film. A strong correlation emerges between ligament size and electrical resistance, which puts forward resistance as an effective parameter for monitoring morphology evolution. Surprisingly, np-Au films with thicker ligaments lead to an increase in electrical resistance, which is unexpected since the extent of charge carrier scattering at the ligament surface should decrease with increasing ligament size. Further examination of np-Au morphology with high-resolution electron microscopy revealed grain growth on the ligaments in highly-annealed np-Au thin films. This suggests that grains act as scattering centers for charge carriers and this becomes the dominant mechanism in dictating electrical resistance in a percolated network of thin conductive ligaments.

### Introduction

Advent of nanotechnology has generated a variety of nanostructured materials with not only enhanced but also previously unknown properties compared to their bulk counterparts.<sup>1-3</sup> These materials (e.g., porous anodic alumina, carbon nanotubes, etc.) have found use in many applications such as biomedical device coatings,<sup>4</sup> data storage devices,<sup>5</sup> thermoelectric materials in energy conversion field,<sup>6</sup> catalysis,<sup>7</sup> and optical sensors.<sup>8</sup> For these materials, the extent and nature of nanostructuring dictates the overall properties, therefore it is crucial to precisely control the nanostructure. This ultimately requires methods and consequently compatible materials, where nanostructure evolution can be both imposed and monitored in a closed-loop manner.

One such emerging material is nanoporous gold (np-Au), which is typically produced by dissolution of silver from a gold-silver alloy, where surface diffusion of gold atoms results in a biocontinuous network of ligaments (Fig. 1A).<sup>9</sup> This material system has found applications in fields such as catalysis,<sup>10</sup> sensors,<sup>11</sup> plasmonics,<sup>8</sup> energy storage,<sup>12</sup> and biomedical devices<sup>13</sup> due to its intriguing properties (e.g., optical,<sup>14</sup> electrical,<sup>15</sup> and mechanical).<sup>16-18</sup> Since all of these properties strongly depend on the nanostructure, numerous methods (e.g., electrochemical,<sup>19</sup> chemical,<sup>20</sup> photo-thermal)<sup>21</sup> have been devised for tuning np-Au morphology, amongst which thermal treatment is the most frequently used. All of these strategies to tune the morphology lead to a coarser yet self-similar pore morphology (Fig. 1B), where the self-similarity is a significant advantage for systematic study of structure-property relationships. However, most of these methods rely on endpoint imaging of the post-treatment morphology, preventing the precise control of the extent of coarsening. We have previously demonstrated *electro-annealing* as a technique for tuning morphology of np-Au thin films, where current flow through the percolated ligament network results in coarsening via a combination

<sup>a</sup>Department of Electrical and Computer Engineering, University of California – Davis, Davis, CA

Email: [eseker@ucdavis.edu](mailto:eseker@ucdavis.edu)

†Electronic Supplementary Information (ESI) available: details on measurement and annealing setup, also resistance calculations and constants used can be found in ESI. See DOI: 10.1039/x0xx00000x

of Joule heating and electron-surface atom interactions.<sup>22</sup> It has been previously reported that resistivity of np-Au depends on its morphology,<sup>15</sup> therefore it should be possible to monitor the morphology evolution of a np-Au thin film while simultaneously using electro-annealing to coarsen it. Taken together, this enables a closed-loop in situ control of coarsening in np-Au thin films. The goal of this paper is to demonstrate this technique and leverage it to investigate the origins of the anomalous electrical resistance changes in np-Au thin films as a function of increasing ligament thickness.

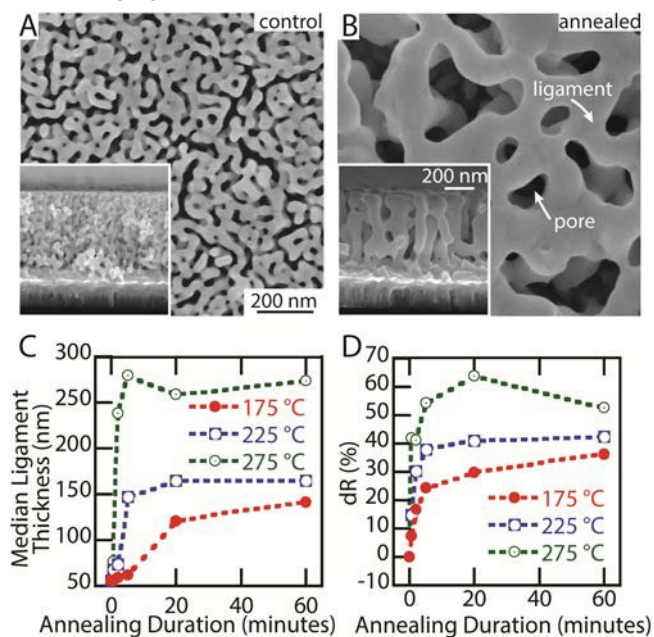


Fig. 1 Top view of an as dealloyed np-Au (control) and annealed np-Au (A and B respectively), cross-sectional view is presented in the insets. C) Median ligament thickness extracted from the SEM images of samples annealed on the hot plate plotted against annealing duration for three different annealing temperatures. D) Resistance change after annealing on the hot plate plotted against annealing duration for three different temperatures (175, 225, 275 °C).

## Materials and Methods

### Chemicals and Materials

Glass coverslips (22 mm x 22 mm) were obtained from Fisher Scientific. Piranha solution, used for sample cleaning, was made by combining 4 parts of hydrogen peroxide (30%) with 1 part sulfuric acid (96%), all by volume. Sputter deposition targets (chrome, gold, and silver of 99.95% purity) were purchased from Kurt J. Lesker. Nitric acid (70%) was purchased from Sigma-Aldrich.

### Sample Preparation

The glass coverslips were cleaned by immersion into a freshly-made piranha solution for 7 minutes. Approximately 120 nm of adhesion chrome layer and 80 nm gold seed layer were sputter-deposited, followed by 500 nm of gold-silver alloy layer. The elemental composition of the alloy was 36% gold and 64% silver (atomic %), as determined by energy dispersive X-ray spectroscopy (Oxford INCA Energy-EDS). The samples were dealloyed in heated nitric acid (55 °C) for 15 minutes and soaked in deionized (DI) water for 2 days to remove residual nitric acid from the porous structure. The samples were diced into 4.4 mm x 22 mm long strips using a laser cutter. Smaller 2 mm x 24 mm samples were fabricated using photolithography as previously described.<sup>22</sup>

### Electro-Annealing Setup

The samples were mounted onto an electro-annealing fixture consisting of PCB board and glass slide. The sample was placed on the glass slide and secured using metal screw-tightened clips. An electrical current from the power supply (DC Power supply 1685B by BK Precision) was injected through the clips into the sample. Temperature was measured with an infrared (IR) thermometer (thermoMETER LS by Micro-Epsilon) positioned above the sample. Voltage across the sample was monitored using a digital oscilloscope (Analog Discovery). Current was obtained directly from the power supply. Power supply, thermometer, and oscilloscope were connected to the computer using USB cables and a custom MatLab code was used for closed-loop temperature control of morphology.

### Image Analysis

Top and cross-sectional images of the samples were obtained using a scanning electron microscope (FEI Nova NanoSEM430). The samples for cross-sectional imaging were prepared by mechanically cleaving the sample along region of interest. SEM images were analyzed by imageJ software and ligament thickness were obtained by custom MatLab code as described in our previous work.<sup>22</sup>

## Results and Discussion

Initially, we investigated the morphology and electrical resistance change in np-Au thin films with samples annealed on a hot plate. Samples were annealed at three different temperatures (175, 225, 275 °C) for 0.5, 2, 5, 20, and 60 minutes. The thin film resistance was measured before and after annealing (Fig. 1D). Typical starting resistance value for a sample with 4.4 mm x 22 mm

dimensions was  $1.98 \pm 0.05 \Omega$ . In order to normalize for baseline resistance variations between samples, unless otherwise indicated, all resistance values are reported as percent change in resistance,  $dR$ , which is defined as  $(R_{\text{post-anneal}} - R_{\text{pre-anneal}}) / R_{\text{pre-anneal}} \times 100$ , where  $R_{\text{pre-anneal}}$  is the resistance of the *as-dealloyed* sample (without any annealing) and  $R_{\text{post-anneal}}$  is the resistance after annealing (measured at room temperature).

Two observations immediately become apparent. First, the amount of steady-state coarsening (quantified as *mean ligament thickness*) is very sensitive to the annealing temperature (Fig. 1C). The primary coarsening mechanism, for temperatures below the melting temperature of gold, is curvature-driven surface diffusion of gold atoms.<sup>21</sup> Above a critical temperature ( $\sim 225^\circ\text{C}$ ), the gold surface atoms diffuse rapidly along the ligaments towards areas with lower curvature. Once a smoother ligament topology (less curvature) is attained, the coarsening process slows down resulting in a porous morphology that is not as sensitive to additional annealing. At this point, a higher temperature is necessary to induce additional coarsening. Fig. 1C illustrates this phenomenon, where a temperature-specific steady-state morphology is reached after approximately 20 minutes of annealing. At lower temperatures ( $<175^\circ\text{C}$ ) annealing still occurs, although it takes significantly longer ( $> 1$  hour) for an appreciable amount of coarsening to become detectable. The second observation, which constitutes the main topic of this paper, is that the trends in Fig. 1C and D indicate that changes in resistance and np-Au morphology (specifically ligament thickness) are related. More specifically, the electrical resistance of the electrode increases with increasing ligament thickness. This relationship is unexpected as thicker ligaments should reduce resistance (to be discussed in the last section). The important finding here is that the electrical resistance can be used as a predictor of morphology change, which has significant utility for in situ control of morphology evolution.

### Closed-Loop Control of Morphology via Electro-Annealing

Since the coarsening is largely dictated by annealing temperature (Fig. 1), annealing on the hot plate is not amenable to precise control of morphology, where the large thermal mass of the hot plate prevents imposing fast modulations in temperature. On the contrary, during electro-annealing the main thermal mass is that of the sample, thereby very precise sample temperatures can be attained rapidly. In addition, since the sample is already electrically-probed for current injection, the electrical properties (i.e., resistance) of the sample can be monitored in situ. Strong correlation between change in

resistance and ligament thickness is illustrated in Fig. 2A, where data from 36 different samples coarsened to various extent were pooled (21 electro-annealed and 15 thermally annealed). Taken together, the electro-annealing is ideally suited to study the relationship between ligament thickness and resistance change during the annealing. It is important to note that thermal and electro-annealing techniques produce similar coarsened morphologies and accompanying resistance changes (Fig. 2A). However, significantly higher temperatures are required for thermal annealing to produce comparable morphologies (see Fig. 2B and C for comparison). The lower temperatures required for electro-annealing to initiate substantial coarsening was attributed to electron-surface atom interactions at high current densities present in the ligaments.<sup>22</sup> Fig. 2A reveals that resistance change as a function of median ligament thickness remains similar for the morphologies produced by traditional thermal annealing and electro-annealing. The inflexion point around 100 nm agrees well with the point where the morphology is no longer similar to the starting morphology (indicative of significant coarsening).

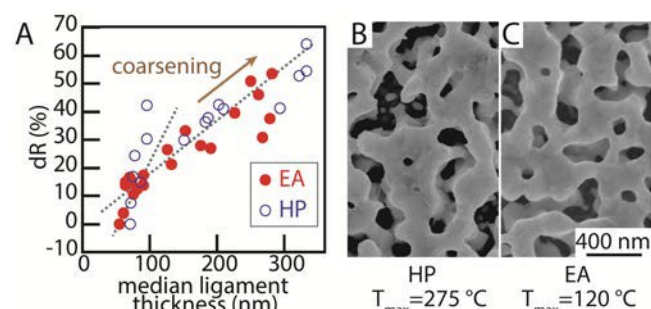


Fig. 2 A) Resistance change versus median ligament thickness for thermally annealed samples (HP) and samples annealed by electro-annealing (EA). B and C) Comparable morphologies obtained by thermal (HP) and electro-annealing (EA) and temperatures required to obtain each morphology.

In order to establish the relationship between electrical resistance and electrode morphology, we first monitored resistance change under electro-annealing at constant temperature. Briefly, the samples were electro-annealed for 60 minutes at constant temperature. The resistance obtained throughout annealing the two samples at  $60^\circ\text{C}$  and  $80^\circ\text{C}$  is shown in Fig. 3A. Pre-annealing resistance was approximately  $1.6 \Omega$  ( $2 \times 24$  mm samples). Initially there is a sharp increase in resistance that is purely temperature dependent, as can be seen in the first 2 minutes of annealing while temperature is being ramped to setpoint (Fig. 3A inset). After the setpoint temperature is reached, any variations to resistance thereafter are attributed to morphological changes. If little or no coarsening occurs, resistance does not increase as can be seen for the  $60^\circ\text{C}$  case. However, at high enough

temperatures when significant coarsening takes place, the resistance increases continuously over the entire annealing duration (as in the 80 °C case). The morphology and electrical resistance were extracted after annealing for all samples. Fig. 3B illustrates the extracted resistance and ligament thickness with respect to the annealing temperature. There was a strong correlation ( $R^2 = 0.95$ ) between the resistance change and ligament thickness. As previously reported, critical temperature of annealing onset is significantly lower compared to the hotplate.

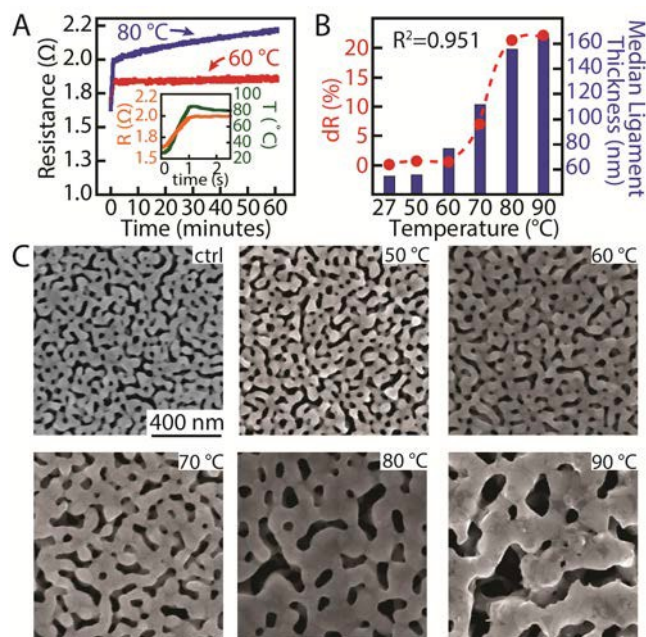


Fig. 3 A) Resistance versus time as samples are electro-annealed at constant temperature mode at 60 and 80 °C. B) Resistance versus temperature and median ligament thickness versus temperature for samples annealed at room, 50, 60, 70, 80, and 90 °C constant temperature mode. C) Corresponding SEM images for the annealed np-Au samples.

Since the electro-annealing setup (Fig. S1A) adjusts the injected current in reference to in situ temperature reading, it is possible to create precise time-varying annealing temperatures. This in turn allows for monitoring resistance change as a function of time-varying annealing temperature. The resistivity of bulk gold increases linearly within the temperature range of interest in this paper (25 °C to 300 °C).<sup>23</sup> Therefore, the resistance of a np-Au sample should also remain linear below the critical temperature for initiating ligament coarsening. We annealed samples while ramping the annealing temperature to three maximum temperatures (80, 100 and 120 °C) for 60 minutes (Fig. 4A). The resistance increased linearly until ~70 °C, after which the slope increased and remained linear for the rest of the temperature range (Fig. 4A). The deviation from the

original slope agrees with the onset of coarsening in np-Au thin films and also signifies that the evolving morphology has significantly coarsened with respect to the starting morphology (Fig. 4B). After the sample cooled down to room temperature, the resistance was re-measured within a temperature range that does not induce annealing (25 °C to 60 °C), as shown in Fig. 4A. For all annealing temperature regimes, the resistance of the sample at room temperature following the annealing cycle was higher than the pre-annealing resistance with the residual resistance increasing with annealing temperature. While the resistance change clearly is due to the change in morphology, it exhibits the opposite trend of what would be expected from coarser wire-like ligaments carrying the current. We hypothesize that an interplay of several mechanisms influence charge transport in np-Au, which is discussed next.

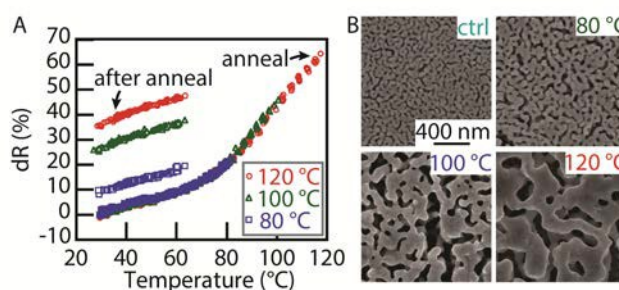


Fig. 4 A) Resistance versus Temperature. Samples were annealed via ramping temperature mode for 60 minutes. Maximum temperatures of 80, 100 and 120 °C test cases are illustrated, where each line represents an average of at least two samples. B) Corresponding SEM images.

### Mechanisms of Resistance Change due to Morphology

Since nanostructured materials constitute a core element of electrical applications (e.g., electrochemical biosensors,<sup>11</sup> fuel cells,<sup>24</sup> and neural electrodes),<sup>13</sup> it is essential to have an understanding of the relationship between electrical resistivity and electrode morphology. The sample resistance was computed assuming that each ligament is a wire that extends an entire length of the sample (Fig. 5A). Thus total resistance is assumed to be a large number of nanowires in parallel. The ligament cross-sectional area was computed using median ligament thickness extracted from SEM images via image processing, and sample dimensions were used for estimating the number of wires (ligaments) that can be stacked in each sample. Film thickness was extracted from SEM images for control, 60, 80, and 90 °C (Fig. 5B i, ii, iii, iv respectively) the remaining film thickness was extrapolated through second order polynomial fit (Fig. S2A). Defect spacing was measured for the samples annealed at 70, 80 and 90 °C directly from the SEM

images (see Fig. 5D). It should be noted that we used the term defect spacing interchangeably with grain size and grain boundary pitch, as these morphological features along with ligament thickness are expected to play the most significant role in interfering with electron transport at this length scale. For the as-dealloyed and slightly annealed samples, the defect spacing was back-calculated using measured resistance, as ligaments are too small to accurately discern defects directly from the SEM images and defects are too far spaced. For the highly-annealed samples, 20 random manual measurements were taken from the SEM images and averaged to obtain the average defect spacing. The chrome and gold seed layers were not included in the resistance calculations, as it is expected that resistance from those layers should not change significantly during annealing. Resistivity was extracted from the resistance using sample dimensions and ligament thickness. Electrical and thermal resistivity are related through Wiedemann-Franz law, which states that electrical and thermal conductivities are related to each other through product of temperature and Lorenz number.<sup>25, 26</sup> Although this relationship does not always hold for nanostructured materials,<sup>27</sup> it has been demonstrated to hold for np-Au.<sup>25</sup> A previous study reported that thermal conductivity of np-Au decreases for thermally-annealed samples with coarser ligaments.<sup>28</sup> Authors argue that in dealloyed np-Au, ligament size is on the order of (or smaller than) mean free path of an electron, thus thermal conductivity is dominated by the contribution of scattering events that occur at the ligament surface. Exposure of np-Au to high temperatures results in formation of thicker ligaments with nanocrystalline sized grains and thermal conductivity becomes increasingly dominated by the contribution of electrons scattering at the grain boundaries. We adopted these findings to compute the thermal conductivity (and consequently electrical conductivity) for samples annealed at constant temperatures in the range of 50 °C to 90 °C in 10 °C increments for 1 hour (Fig. 3C). Thermal conductivity for each ligament was computed using,<sup>28</sup>

$$\lambda_s = \frac{1}{3} v_F^2 \frac{\gamma T}{AT^2 + BT + v_F/d_{an} + v_F/l_{an}^*}$$

where  $v_F$  is Fermi velocity,  $d_{an}$  is median ligament thickness,  $AT^2$  is reciprocal of the electron-electron scattering time,  $BT$  is reciprocal of electron-phonon scattering time,  $v_F/d_{an}$  is reciprocal of electron-surface scattering time, and  $v_F/l_{an}^*$  is the reciprocal of the electron-defect scattering. Also,  $l_{an}^* = l_{an} \cdot (1-\Gamma)/\Gamma$  where  $l_{an}$  is mean defect spacing and  $\Gamma$  is electron reflection coefficient, for all calculations  $\Gamma$  was taken as 0.3.<sup>28</sup> The numerical definitions of  $v_F$ ,  $\gamma$ ,  $A$ , and  $B$  can be found in Table S2. This formula takes into account the effect of

electron scattering from ligament surface as well as contributions from defects such as grain boundaries. As shown in Fig. 5C, initial estimates using resistivity with no defects (by setting  $v_F/l_{an}^*$  to zero in the equation above) predict that resistance should decrease with increasing ligament thickness as expected. However, resistance starts to increase once defects are introduced. For comparison we also plotted how resistance changes by increasing and decreasing defect spacing by one standard deviation below and above the average defect spacing. As expected, the electrical resistance is extremely sensitive to this parameter and plays the dominant role in dictating resistance of the nanoporous structure (Fig. 5C and S3). The increase in defect spacing with annealing is attributed to formation of thicker multi-grain ligaments during the coarsening process.<sup>29, 30</sup> Finally, it should be noted that the model becomes less accurate for the cases of excessive coarsening (e.g., 90 °C case), where the ligament thickness becomes comparable to the film thickness and the material becomes less isotropic.

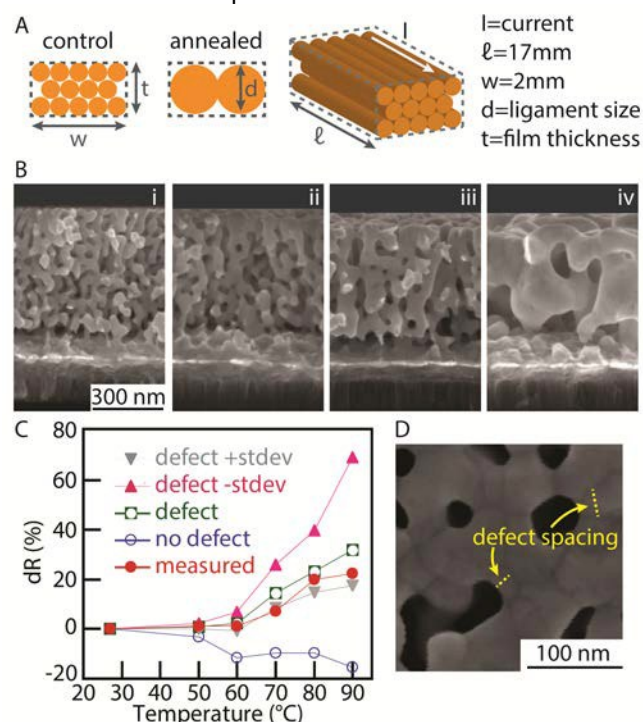


Fig. 5 A) Illustration of the physical wire model of np-Au structure used for calculating the resistance of np-Au thin films with different morphologies. B) Cross-sectional SEM images showing np-Au thickness reduction after annealing (i: control, ii: 60 °C, iii: 80 °C, iv: 90 °C). Thickness was extracted and used in resistance calculations ( $t$  = film thickness). C) Measured (*measured* label) and computed percent change in resistance after annealing at different temperatures. Resistance was computed without defects (*no defect* label), resistance with defects (*defect* label) was calculated using measured defect spacing. Finally, the sensitivity of resistance due to variation in defect spacing is shown via the resistance computed using the measured defect spacing  $\pm$  one

standard deviation. D) SEM image illustrating defect spacing in an annealed sample.

## Conclusion

We used electro-annealing to investigate the relationship between coarsening and resistance changes in annealed np-Au samples, which is an emerging material for biomedical and energy applications, as well as model system for fundamental material science studies. All of these applications require precise control of morphology. In comparison to other annealing techniques (e.g., thermal treatment), electro-annealing is amenable to in situ modulation and monitoring of morphology evolution, low-temperature coarsening, and isolated annealing of electrically separate np-Au traces on a single substrate. These single-chip multiple-morphology libraries are expected to facilitate high-throughput structure-property relationship studies for identifying optimal morphologies for different applications. Our work here revealed that electrical resistance of np-Au electrodes increases with coarsening due to the growth of grains (defects) that act as scattering sites that hinder electronic transport through the ligaments. The defect density played a dominant role in dictating the electrical resistance compared to the coarsening of ligaments that facilitate electronic transport by reducing electron-surface scattering events. We expect this electrical monitoring technique to not only allow for monitoring morphology evolution in nanoporous metals with high surface mobility (that is, tendency to coarsen), but also serve as a tool to monitor defect nucleation and growth in materials with percolated conductive paths.<sup>22</sup>

## Acknowledgement

We gratefully acknowledge support from UC Lab Fees Research Program Award [12-LR-237197], Research Investments in the Sciences & Engineering (RISE) Award and National Science Foundation Grants [CBET-1512745 and CBET&DMR-1454426].

## References

- 1 R. Z. Valiev, M. J. Zehetbauer, Y. Estrin, H. W. Höppel, Y. Ivanisenko, H. Hahn, G. Wilde, H. J. Roven, X. Sauvage and T. G. Langdon, *Advanced Engineering Materials*, 2007, **9**, 527-533.
- 2 H. Gleiter, *Acta Materialia*, 2000, **48**, 1-29.
- 3 M. Cain and R. Morrell, *Applied Organometallic Chemistry*, 2001, **15**, 321-330.
- 4 E. Martínez, E. Engel, J. A. Planell and J. Samitier, *Annals of Anatomy - Anatomischer Anzeiger*, 2009, **191**, 126-135.
- 5 J.-S. Lee, *Journal of Materials Chemistry*, 2011, **21**, 14097-14112.
- 6 C. J. Vineis, A. Shakouri, A. Majumdar and M. G. Kanatzidis, *Advanced Materials*, 2010, **22**, 3970-3980.
- 7 J. Biener, M. M. Biener, R. J. Madix and C. M. Friend, *ACS Catalysis*, 2015, **5**, 6263-6270.
- 8 J. Qi, J. Zeng, F. Zhao, S. H. Lin, B. Raja, U. Strych, R. C. Willson and W.-C. Shih, *Nanoscale*, 2014, **6**, 8521-8526.
- 9 J. Erlebacher, M. J. Aziz, A. Karma, N. Dimitrov and K. Sieradzki, *Nature*, 2001, **410**, 450-453.
- 10 A. Wittstock, J. Biener and M. Baumer, *Physical Chemistry Chemical Physics*, 2010, **12**, 12919-12930.
- 11 P. Daggumati, S. Appelt, Z. Matharu, M. L. Marco and E. Seker, *Journal of the American Chemical Society*, 2016, **138**, 7711-7717.
- 12 X. Y. Lang, H. T. Yuan, Y. Iwasa and M. W. Chen, *Scripta Materialia*, 2011, **64**, 923-926.
- 13 C. A. R. Chapman, H. Chen, M. Stamou, J. Biener, M. M. Biener, P. J. Lein and E. Seker, *ACS Applied Materials & Interfaces*, 2015, **7**, 7093-7100.
- 14 M. M. P. Arnob, F. Zhao, J. Zeng, G. M. Santos, M. Li and W.-C. Shih, *Nanoscale*, 2014, **6**, 12470-12475.
- 15 T. Fujita, H. Okada, K. Koyama, K. Watanabe, S. Maekawa and M. W. Chen, *Physical Review Letters*, 2008, **101**, 166601.
- 16 D. Lee, X. Wei, X. Chen, M. Zhao, S. Jun, J. Hone, E. Herbert, W. Oliver and J. Kysar, *Scripta Materialia*, 2007, **56**, 437-440.
- 17 H. J. Jin and J. Weissmüller, *Science*, 2011, **332**, 1179-1182.
- 18 E. Detsi, S. Punzhin, J. Rao, P. R. Onck and J. T. M. De Hosson, *ACS Nano*, 2012, **6**, 3734-3744.
- 19 A. Sharma, J. Bhattarai, K. A. Alla, J. A. Demchenko, V. and J. S. Keith, *Nanotechnology*, 2015, **26**, 085602.
- 20 M. Hakamada and M. Mabuchi, *Materials Letters*, 2008, **62**, 483-486.
- 21 C. A. R. Chapman, L. Wang, J. Biener, E. Seker, M. M. Biener and M. J. Matthews, *Nanoscale*, 2016, **8**, 785-795.
- 22 T. S. Dorofeeva and E. Seker, *Nano Res.*, 2015, **8**, 2188-2198.
- 23 R. A. Matula, *Journal of Physical and Chemical Reference Data*, 1979, **8**, 1147-1298.
- 24 A. S. Arico, P. Bruce, B. Scrosati, J.-M. Tarascon and W. van Schalkwijk, *Nat Mater*, 2005, **4**, 366-377.
- 25 X. Re, W. Jian Li, W. Rongyue, L. Xide, Z. Xing, F. Xi-Qiao and D. Yi, *Nanotechnology*, 2010, **21**, 085703.
- 26 A. J. Minnich, M. S. Dresselhaus, Z. F. Ren and G. Chen, *Energy & Environmental Science*, 2009, **2**, 466-479.
- 27 Q. G. Zhang, B. Y. Cao, X. Zhang, M. Fujii and K. Takahashi, *Physical Review B*, 2006, **74**, 134109.
- 28 J. Wang, R. Xia, J. Zhu, Y. Ding, X. Zhang and Y. Chen, *Journal of Materials Science*, 2012, **47**, 5013-5018.
- 29 J. Erlebacher, *Physical Review Letters*, 2011, **106**, 225504.
- 30 Y.-c. K. Chen-Wiegart, S. Wang, Y. S. Chu, W. Liu, I. McNulty, P. W. Voorhees and D. C. Dunand, *Acta Materialia*, 2012, **60**, 4972-4981.